Molecular Imaging of Temporal Dynamics and Spatial Heterogeneity of Hypoxia-Inducible Factor-1 Signal Transduction Activity in Tumors in Living Mice

Inna Serganova,[1] Michael Doubrovin,[1] Jelena Vider,[2] Vladimir Ponomarev,[2] Suren Soghomonyan,[5] Tatiana Beresten,[1] Ludmila Ageyeva,[1] Alexander Serganov,[4] Shangde Cai,[3] Julius Balatoni,[5] Ronald Blasberg,[1,2] and Juri Gelovani[1,2,5]

[1]Department of Neurology, [2]Department of Radiology, [3]Radiochemistry/Cyclotron Core Facility, and [4]Structural Biology Program, Memorial Sloan-Kettering Cancer Center, New York, New York; and [5]Experimental Diagnostic Imaging, M. D. Anderson Cancer Center, Houston, Texas

ABSTRACT

Tumor hypoxia is a spatially and temporally heterogeneous phenomenon, which results from several tumor and host tissue-specific processes. To study the dynamics and spatial heterogeneity of hypoxia-inducible factor-1 (HIF-1)-specific transcriptional activity in tumors, we used repetitive noninvasive positron emission tomography (PET) imaging of hypoxia-induced HIF-1 transcriptional activity in tumors in living mice. This approach uses a novel retroviral vector bearing a HIF-1–inducible "sensor" reporter gene (HSV1-tk/GFP fusion) and a constitutively expressed "beacon" reporter gene (DsRed2/XPRT). C6 glioma cells transduced with this multireporter system revealed dose-dependent patterns in temporal dynamics of HIF-1 transcriptional activity induced by either CoCl$_2$ or decreased atmospheric oxygen concentration. Multicellular spheroids of C6 reporter cells developed a hypoxic core when >350 μm in diameter. ^{18}F-2′-fluoro-2′deoxy-1β-D-arabionofuranosyl-5-ethyl-uracil (FEAU) PET revealed spatial heterogeneity of HIF-1 transcriptional activity in reporter xenografts in mice as a function of size or ischemia-reperfusion injury. With increasing tumor diameter (>3 mm), a marked increase in HIF-1 transcriptional activity was observed in the core regions of tumors. Even a moderate ischemia-reperfusion injury in small C6 tumors caused a rapid induction of HIF-1 transcriptional activity, which persisted for a long time because of the inability of C6 tumors to rapidly compensate acute changes in tumor microcirculation.

INTRODUCTION

Hypoxia is one of the key factors influencing tumor progression and resistance to therapy by inducing various metabolic, molecular-genetic, and pathophysiologic adaptive processes, including neoangiogenesis. Tumors become hypoxic because rapidly proliferating tumor cells outgrow their blood supply. The newly developing neoangiogenic blood vessels are aberrant and unable to sustain adequate blood flow, which contributes to regional tissue hypoxia and the development of pathophysiologic *circulus viciousus.* Tumor hypoxia is spatially and temporally heterogeneous phenomenon that results from a combination of factors, including tumor site, regional microvessel density, blood flow, oxygenation level, tumor type, proliferative activity, metabolism, and aberrations of hypoxia-sensitive or hypoxia-responsive signaling pathways in tumor cells. A convergence for these factors is the hypoxia-signaling pathway and involves hypoxia-inducible transcription factor-1 (HIF-1). HIF-1 is a heterodimeric protein composed of two subunits: a constitutively expressed HIF-1β and the α-subunit (1). During normoxia, HIF-1α is rapidly degraded by ubiquitination, whereas exposure to hypoxic conditions prevents its degradation (2). The enzymatic hydroxylation of proline-564 and -603 of HIF-1α controls the turnover of the protein

by tagging it for interaction with the von Hippel-Lindau protein (3). Under hypoxic conditions, HIF-1α level is increased and it forms a complex with HIF-1β and the CBP/p300 coactivator (4) and translocates into the nucleus, where it binds to the core DNA sequence 5′-RCGTG-3′ (5). Many oncogenic signaling pathways overlap with the HIF-1 signaling pathway (6, 7) and cause up-regulation of many HIF-1–inducible genes [*e.g.,* vascular endothelial growth factor (VEGF), erythropoietin, and glucose transporters] and several glycolytic enzymes even under normoxic conditions (8).

The lack of technologies for quantitative noninvasive imaging of the dynamics and spatial heterogeneity of HIF-1–specific transcriptional activity in experimental tumor models *in vivo* is a significant impediment for conducting such studies. To address this problem, we have developed an approach that allows for repetitive noninvasive positron emission tomography (PET) imaging of hypoxia-induced HIF-1 transcriptional activity in tumor xenografts in living mice. It is based on technology for noninvasive imaging of a reporter gene expression with PET (9). We previously used a similar approach to noninvasively image transcriptional regulation of endogenous gene expression by p53 (10) and nuclear factor of activated T cells (NFAT; ref. 11). Other investigators also have used this *HSV1-tk*–based PET imaging approach for noninvasive monitoring of transcriptional regulation of endogenous genes via prostate-specific antigen (12) and human elongation factor-1α (13) promoters, for visualization of p53 and large T-antigen protein-protein interactions in tumor xenografts *in vivo* (14), and for imaging the regulation of albumin expression in transgenic mice (15).

For the current studies, we developed a novel retroviral vector bearing a dual reporter gene cassette for stable transduction of tumor cells with an HIF-1–inducible "sensor" and a constitutively expressed "beacon" reporter gene. In C6 rat glioma cells, we quantitatively characterized the dose-dependent differences in temporal dynamics of HIF-1 transcriptional activity using chemically induced hypoxia (with CoCl$_2$) and decreased atmospheric oxygen. We showed that HIF-1–mediated activation of *TKGFP* reporter gene expression in hypoxic tumor tissue can be noninvasively and repeatedly visualized in living mice using PET imaging with [^{18}F]2′-fluoro-2′deoxy-1β-D-arabionofuranosyl-5-ethyl-uracil (FEAU).

MATERIALS AND METHODS

Generation of *cis*-HRE/tkGFP Vectors. The retroviral vector dxNFAT-TKGFP-Neo (11) with deletion of the viral enhancer in 3′-LTR was used as the backbone. First, the neomycin resistance gene was replaced with a hybrid reporter fusion Red2XPRT (16) to be constitutively expressed from cytomegalovirus (CMV) promoter. The NFAT enhancer then was replaced with the cDNA fragment bearing eight repeats of the hypoxia-responsible element (HRE; 5′-GCCCTACGTGCTGTCTCACACAGC-3′) from the 3′ enhancer region of human *Epo* gene to drive the expression of TKGFP (17). The dxHRE-tk/eGFP-cmvRed2XPRT plasmid (Fig. 1*A*) was transfected into the GPG293 transient retroviral producer cells (18) using LipofectAMINE 2000 (Invitrogen, Carlsbad, CA).

Tumor Cells and Transduction. The C6 rat glioma cell line was obtained from American Type Culture Collection (Manassas, VA). The cells were transduced with newly generated retroviral vector by incubating 50% confluent
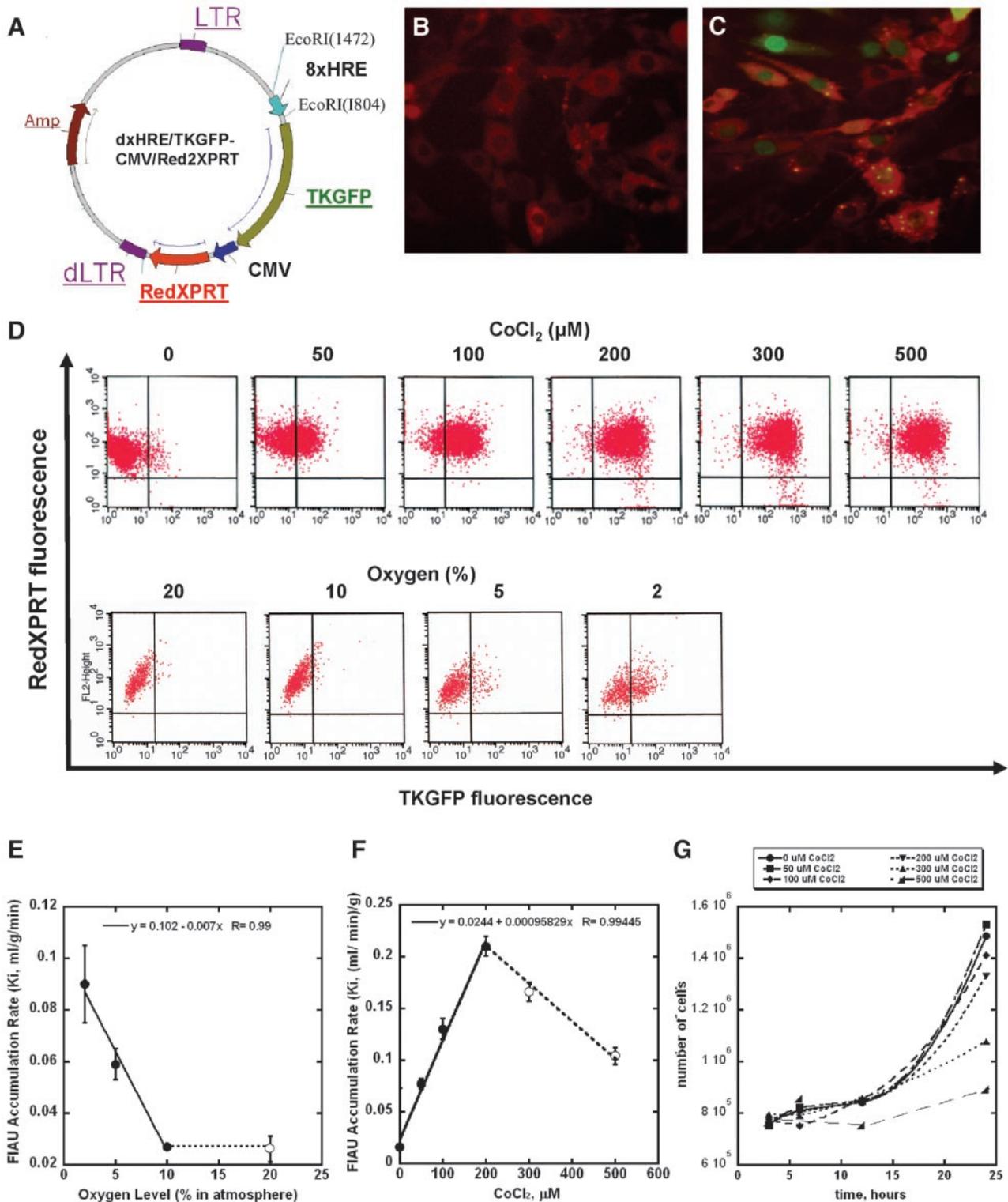
Fig. 1. Characterization of hypoxia-sensitive specific reporter system *in vitro*. Structural schema of the dxHRE/TKGFP-CMV/Red2XPRT retroviral vector-encoding plasmid (*A*). Fluorescence microscopy of #4C6 reporter cells under baseline conditions (*B*) and following exposure to 200 μmol/L CoCl$_2$ for 24 hours (*C*). Two-color FACS analyses of #4C6 cells exposed to different concentrations of CoCl$_2$ in the medium or low atmospheric oxygen for 24 hours; the constitutive dsRFP2/XPRT fluorescence is shown on the ordinate, and inducible HRE-TKGFP fluorescence is shown on the abscissa (*D*). The rate of [^{14}C]FIAU accumulation (a measure of TKGFP expression) in #4C6 reporter cells following a 24-hour exposure to different concentrations of atmospheric oxygen (*E*) or CoCl$_2$ (*F*). *In vitro* growth profiles of #4C6 cells in culture medium with different CoCl$_2$ concentrations (*G*).

tumor cells with the virus-containing medium for 12 hours in presence of Polybrene (8 μg/mL; Sigma, St. Louis, MO).

Cell Cultures and Hypoxia Induction. The C6-dxHRE-TKGFP-cmvRed2XPRT cells were plated in 16.5-cm dishes (NUNC, Roskilde, Denmark) and maintained under normoxic (5% CO$_2$, 20% O$_2$, and 75% N$_2$) or hypoxic conditions in humidified atmosphere at 37°C (NU-4950; NuAire Inc.,

Plymouth, MN). Hypoxic conditions (2%, 5%, or 10% of O$_2$) were achieved by precisely calibrated cycles of gassing of the incubator chambers with N$_2$ and 5% CO$_2$.

Selection of Transduced Tumor Cell Clones. The C6-dxHRE-TKGFP-cmvRed2XPRT cell population was selected using fluorescence-activated cell sorter (FACS; BD Bioscience, San Jose, CA) based on constitutive expression

6102

of RedX2PRT and no expression of TKGFP reporter proteins. The selected RedX2PRT$^+$, TKGFP$^-$ cells were treated with 200 μM of CoCl$_2$ for 24 hours to induce TKEGFP expression. The cell population expressing Red2XPRT$^+$ and TKGFP$^+$ at high levels was selected using FACS. The selected Red2XPRT$^+$, TKGFP$^+$ population of cells was "rested" in regular medium for 2 or 3 days, and the Red2XPRT$^+$ but TKGFP$^-$ (negative) population again was reselected. This cycle of negative selection–induction–positive selection–rest–negative selection was repeated three times to obtain a highly sensitive and maximally inducible cell population with minimal background activity of the reporter system.

To warrant the stability of performance of the reporter cells, single cell-derived clones were obtained from selected reporter cell population. The clone #4C6-dxHRE-TKGFP-cmvRed2XPRT with the highest level of TKGFP expression was selected for further studies, and later throughout this report, the #4C6-dxHRE-TKGFP-cmvRed2XPRT cells will be referred as "#4C6 reporter cells."

Radiotracer Assay for TKGFP Expression *In vitro*. *In vitro* radiotracer accumulation studies with [^{14}C] 2′-fluoro-2′deoxy-1β-D-arabionofuranosyl-5-iodo-uracil (FIAU) were performed as described previously (9, 19). These radiotracer uptake studies were performed in the #4C6 reporter cells with CoCl$_2$ or under different levels of oxygen.

Assessment of VEGF Concentration in Cell Culture Medium. The #4C6 reporter cells were seeded at 1.5×10^5 cells/dish in DMEM. Cells were cultured with or without the CoCl$_2$ in the culture medium; conditioned media samples were collected at different time points, centrifuged, and assayed by ELISA using the Quantikine VEGF immunoassay kit (R&D Systems, Minneapolis, MN), which recognizes rat and murine VEGF164 and VEGF120 isoforms. The measured concentrations of VEGF in conditioned cell culture medium were normalized by the total amount of protein measured in tumor cells in corresponding cultures (pg VEGF/mg protein in cells).

Assessment of HIF-1 Transcriptional Activity in Cells. The level of HIF-1 transcriptional activity was assessed under normoxia, hypoxia, or after CoCl$_2$ treatment. The levels of transcriptionally active HIF-1α complexes were measured using the ELISA-based kit from the nuclear extracts of #4C6 reporter cells (Active Motif North America, Carlsbad, CA).

Three-Dimensional Spheroid Cultures. Multicellular spheroids were generated in 96-well V-bottomed plates (Costar, Cambridge, MA), and 3×10^3 #4C6 reporter cells were placed into each well and centrifuged at 2000 rpm for 5 minutes. After 24 hours of incubation, the individual spheroids were transferred into 96-well flat-bottomed plates for daily microscopic monitoring of their growth using an LSM 510 confocal microscope (Zeiss, Oberkochen, Germany).

Animal Studies. Animal study protocols were approved by the Memorial Sloan-Kettering Institutional Animal Care and Use Committee. Two groups of immune-compromised *nu/nu* mice (Harlan, Indianapolis, IN) weighing 20 grams on average were used to develop *in vivo* models of tumor tissue hypoxia. The first group was used to study tumor hypoxia that develops in tumor tissue as the result of tumor outgrowing its blood supply. Three #4C6 reporter cell tumors were implanted on the left side, and three control wild-type C6 tumors were implanted on the right side. Different numbers of corresponding tumor cells were injected in each of these sites to generate xenografts of different sizes: 5×10^5 cells were implanted in the shoulder area to produce large tumors; 1.5×10^5 cells were implanted in the middle dorsal-lateral area to produce medium-sized tumors; and 5×10^4 cells were implanted in the thigh to produce small tumors. The size was measured in two dimensions using calipers, and tumor volume was calculated as V = length $\times$ width^2 $\times$ 0.5.

Another group of animals was used to study the development of acute hypoxia as a result of temporary circulatory arrest (ischemia-reperfusion injury model). The #4C6 reporter cells (0.3×10^6) were injected s.c. into the dorsal aspects of both anterior limbs of mice, and small (25 ± 4.0 mm^3) s.c. tumors had developed 10 days later. At that point, the animals were imaged to determine baseline levels of expression of the TKGFP reporter. To temporary block the blood flow to the s.c. tumor, a tourniquet was applied for 1 hour proximally to the tumor on the left anterior limb; the right tumor-bearing limb was unaffected and served as a control. PET imaging was performed the next day after the tourniquet applications.

[^{18}F]FEAU Synthesis and PET Imaging. [^{18}F]FEAU was synthesized using a modified no-carrier added procedure described by Alauddin *et al.* (20) for synthesis of [^{18}F] 2′-fluoro-2′deoxy-1β-D-arabionofuranosyl-5-methyl-uracil (FMAU). Freshly prepared 2,4-bis-*O*-(trimethylsilyl)-5-ethyluracil for condensation with the radiosynthetic intermediate 2′-deoxy-2′-[^{18}F]fluoro-3,5-di-*O*-benzoyl-α-D-arabinofuranosyl bromide was used to produce [^{18}F]FEAU. Mice were administered [^{18}F]FEAU (i.v. 100 μCi/animal). Body PET was performed using a microPET R4 (Concorde Microsystems, Knoxville, TN). Images were acquired for 10 minutes under inhalation anesthesia (isoflurane 2%). The level of radioactivity in tumors (% dose/g) was estimated from images as described previously by our group (9–11).

Fluorescence Imaging *In situ*. After the last PET imaging session, the animals were sacrificed, and whole s.c. #4C6 reporter cell xenografts were excised and frozen in the OCT embedding matrix (Shandon Lipshaw, Inc, Pittsburgh, PA). Frozen tissue sections (20 μm) were obtained with the OTF cryomicrotome (Bright-Hacker, Fairfield, NJ), fixed in ice-cold methanol for 10 minutes, and washed with PBS. Methanol fixation preserves green fluorescent protein (GFP) fluorescence while significantly reducing the background tissue fluorescence. Normoxic (red) and hypoxic (red + green) tumor cells and were visualized with the Eclipse TS100 digital fluorescence microscope system (Nikon, Tokyo, Japan).

RESULTS

Characterization of Hypoxia Sensitive HIF-1–Specific Reporter System *In vitro*. Single cell-derived #4C6 reporter cells were selected using FACS based on constitutive expression of Red2XPRT and low background levels of HRE-regulated TKGFP expression. Fluorescence microscopic examination of #4C6 reporter cells showed an adequate level of Red2XPRT and almost negligible levels of TKGFP expression under normoxia (Fig. 1*B*). To assess the responsiveness of the HIF-1–sensitive part of the reporter system, hypoxic conditions were initially modeled by exposing #4C6 cells to culture medium with 200 μmol/L CoCl$_2$ for 24 hours. Such conditions induced the expression of TKGFP reporter protein in cell nuclei, whereas the cytoplasm of cells continued to show red fluorescence because of constitutive expression of Red2XPRT reporter protein (Fig. 1*C*). Sixty-fold induction of TKGFP fluorescence was observed in the cell population after treatment with 200 μmol/L CoCl$_2$ as measured by FACS (Fig. 1*D*).

Additional studies showed that the up-regulation of TKGFP reporter expression in #4C6 cells was CoCl$_2$ concentration dependent and saturable at concentrations >200 to 300 μmol/L CoCl$_2$ (Fig. 1*D*). It is noteworthy that at these high concentrations of CoCl$_2$, a small population of cells (~5%) with characteristic loss of Red2XPRT reporter expression was observed. Up-regulation of TKGPF expression was oxygen dependent (Fig. 1*D*). Comparable levels of reporter expression were observed at 50 μmol/L CoCl$_2$ and 2% atmospheric oxygen.

A radiotracer assay also was used to assess the relationship between different levels of atmospheric oxygen or CoCl$_2$ in the medium and TKGFP reporter expression. TKGFP-mediated accumulation of [^{14}C]FIAU for 2 hours was measured in #4C6 cells under normoxic conditions and after 24-hour exposure to different concentrations of CoCl$_2$ in the medium or oxygen in the atmosphere. A fourfold increase in the rate of [^{14}C]FIAU accumulation was observed after 24-hour exposure of #4C6 cells to 2% atmosphere oxygen, the lowest concentration tested. This increase in TKGFP enzymatic activity was linear ($r = 0.99$) between 10% and 2% atmospheric oxygen (Fig. 1*E*). The threshold of hypoxic induction of TKGFP expression in #4C6 reporter cells was observed at 10% oxygen based on FACS and [^{14}C]FIAU accumulation studies.

The net accumulation rate (K_i) of [^{14}C]FIAU increased in a CoCl$_2$ concentration-dependent manner, and the increase was linear ($r = 0.99$) up to 200 μmol/L CoCl$_2$ (Fig. 1*F*). A 10-fold increased rate of [^{14}C]FIAU accumulation (TKGFP enzymatic activity) was observed at 200 μmol/L CoCl$_2$. Above 200 μmol/L CoCl$_2$, the rate of [^{14}C]FIAU accumulation decreased, which probably reflects to
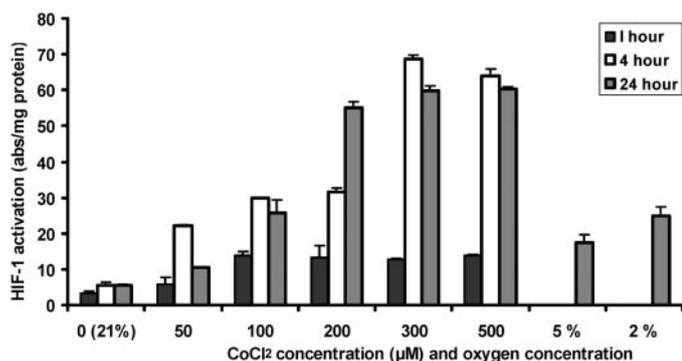
6103

Fig. 2. HIF-1α transcription complex activity. Measurements of transcriptionally active HIF-1α complexes were performed using an ELISA-based assay in nuclear extracts of #4C6 cells exposed for various periods to different CoCl₂ (in medium) or atmospheric oxygen concentrations.

$CoCl_2$-induced toxicity. Toxicity was confirmed by a significant inhibition of tumor cell proliferation observed at $CoCl_2$ concentrations >200 μmol/L (Fig. 1*G*).

Transcriptional Activation of HIF-1 under Various Hypoxia Conditions. Experiments were performed to verify that up-regulation of TKGFP reporter is the result of increased HIF-1 transcriptional activity. The $CoCl_2$ concentration-dependent kinetics of HIF-1 transcriptional activation was assessed in #4C6 cells *in vitro* using an ELISA-based assay for quantitation of transcriptionally active HIF-1α complexes from cell nuclear extracts.

HIF-1 transcriptional activity increased as early as 1 hour after exposure of #4C6 cells to various (50 to 500 μM) $CoCl_2$ concentrations (Fig. 2). A fivefold increase in HIF-1 transcription was achieved with 100 μM $CoCl_2$, and the maximum increase in HIF-1 (~10-fold) occurred after 4-hour treatment with 100 μM $CoCl_2$ and at 24 hours starting from 200 μM $CoCl_2$. Similar high levels of HIF-1 transcription were observed after 4- and 24-hour exposure at the 300 and 500 μM $CoCl_2$ concentrations. Interestingly, at 50 μM $CoCl_2$, the HIF-1 transcriptional activity was lower at 24 hours than that at 4 hours.

The transcriptional level of HIF-1 also was measured after exposure of #4C6 cells to reduced oxygen concentrations (Fig. 2). At a hypoxia level of 2% oxygen, HIF-1 transcription enhanced only threefold after 24-hour exposure and was similar to the 4-hour level of induction by 50 μM $CoCl_2$. These levels also correspond with the induction of

TKGFP reporter protein, as measured by FACS analysis and [¹⁴C]FIAU accumulation assays (Fig. 1*D* and *E*).

Dose-Dependent Kinetics of TKGFP Production and VEGF Secretion. To compare dose-dependent responses of the hypoxia-sensitive reporter system to the dynamics of endogenous VEGF secretion, we determined levels of VEGF protein concentration (murine VEGF164 and VEGF120 forms) in the culture medium of reporter cells at various $CoCl_2$ concentrations (0 to 500 μM) during 24 hours of incubation. The concentration of VEGF in the cell culture medium increased over time for each tested concentration of $CoCl_2$ (Fig. 3*A*). The measured VEGF concentrations were normalized by the total amount of protein in cells in corresponding cultures (pg VEGF/mg protein cells) and plotted against time of sampling. The rate of increase in VEGF concentration over time (slope) was determined for each $CoCl_2$ concentration using a linear regression analysis and was used as a measure of an "apparent" rate of VEGF secretion into the medium (pg VEGF/mg protein cells/h), which is not corrected by the rate of VEGF degradation. When the measures of an apparent rate of VEGF secretion were plotted against the corresponding $CoCl_2$ concentrations a linear relationship were observed up to 300 μM $CoCl_2$ (Fig. 3*C*). The decline in the apparent rate of VEGF secretion at 500 μM $CoCl_2$ probably was because of cell toxicity (Fig. 1*F*).

A similar $CoCl_2$ concentration-dependent increase was observed in the percent of TKGFP-expressing #4C6 cells, as estimated by FACS of cell cultures from which the VEGF samples were obtained and assayed (Fig. 3*B*). The percent of TKGFP-expressing cells increased linearly during the first 13 to 14 hours of $CoCl_2$ treatment, and when the rate of increase (slope) was plotted against the corresponding concentration of $CoCl_2$ (Fig. 3*B*), a linear relationship was observed between 0 and 300 μM $CoCl_2$ (Fig. 3*C*), which paralleled the relationship observed for VEGF secretion rates.

Size-Dependent Heterogeneity of HIF-1 Transcriptional Activity in Multicellular #4C6 Spheroids. Multicellular spheroids were grown from #4C6 cells in regular culture medium under normoxic conditions and imaged with a confocal laser microscope at different stages of growth (Fig. 4). When #4C6 spheroids were <300 μm in diameter, the cells showed only red fluorescence caused by constitutive expression of Red2XPRT reporter; the hypoxia-inducible TKGFP green fluorescence was not detectable (Fig. 4*A*). After #4C6 spheroids reached ~350 to 400 μm in diameter, hypoxia-induced TKGFP green fluorescence was clearly observed inside the core region of spheroids (Fig. 4*B* and *C*). Once hypoxia developed, the thickness of nonhy-
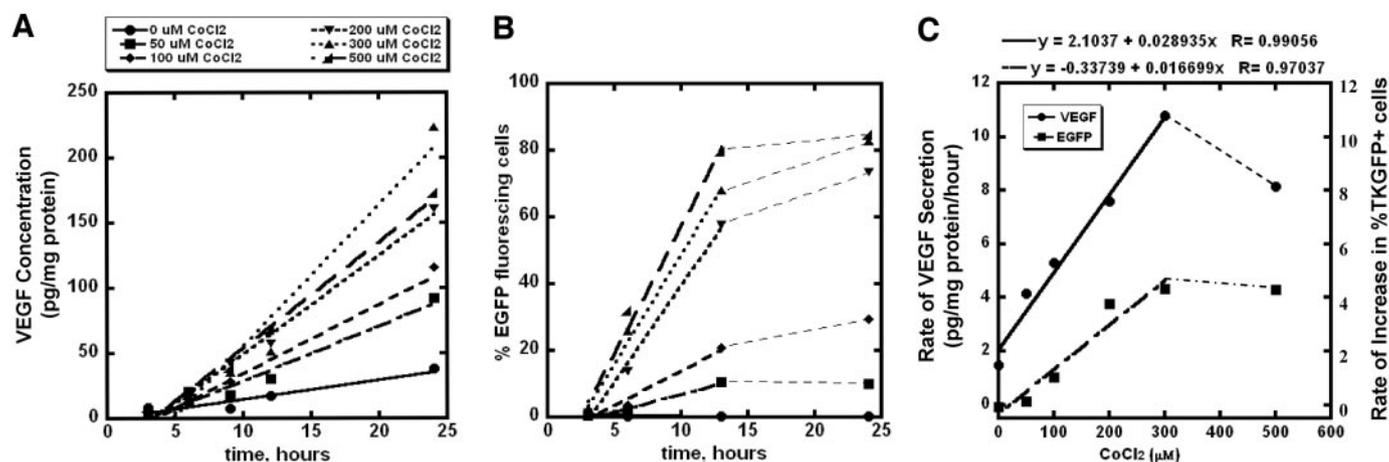

Fig. 3. Dose-dependent kinetics of TKGFP production and VEGF secretion. ELISA-based measurements of VEGF concentration in #4C6 culture medium over time containing different concentrations of CoCl₂ (*A*). Two-color FACS-aided assessments of TKGFP-fluorescing cells (% of total) in the same cell cultures (*B*). From the plot *A,* the linear regression fits ("apparent" rates of VEGF secretion) were plotted *versus* corresponding CoCl₂ concentrations (*C,* left ordinate). The slopes of linear portions of data in plot *B* were calculated to show different increase rates in number of TKGFP fluorescing cells at various CoCl₂ concentrations (*C,* right ordinate).
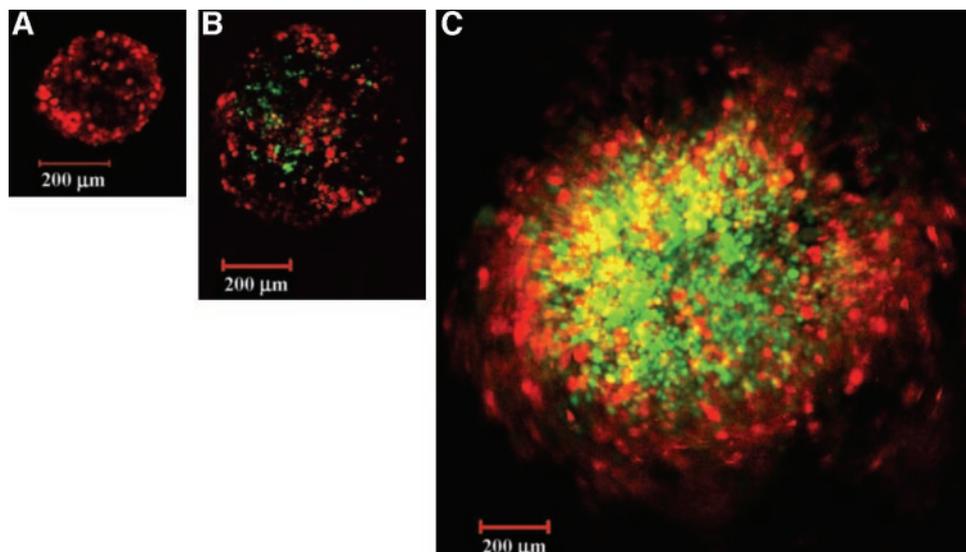
6104

Fig. 4. Development of hypoxia in multicellular #4C6 spheroids. Sequential confocal microscopic images of the same #4C6 multicellular spheroid during different phases of growth; *bar,* 200 μm. Normoxic spheroid with no HIF-1 transcriptional activity and only constitutive red-fluorescing cells (*A*). Hypoxic TKGFP-fluorescing cells are clearly detectable within the central region when the spheroid grows to 350 to 400 μm in diameter (*B*). At a significantly larger size, this central region becomes significantly more hypoxic as evidenced by the increased number of TKGFP-fluorescing cells (*C*).

poxic "shell," 82 $\pm$ 21 μm in average, remained unchanged. The nonhypoxic shell in the larger spheroids also harbored a small number of hypoxia-induced TKGFP-expressing #4C6 reporter cells, which sometimes were observed even in the outmost cellular layers (Fig. 4*C*).

Noninvasive Imaging of HIF-1 Transcriptional Activity in Tumors of Various Sizes. The first group of mice ($n = 6$) was used to study tumor hypoxia that develops in tumor tissue as a function of tumor size that outgrows its blood supply. This experiment represents an *in vivo* extension of the *in vitro* spheroid study. Different numbers of wild-type C6 or #4C6 cells were injected s.c. in different areas of the mouse body (see Materials and Methods). Three weeks after implantation, these cells developed s.c. xenografts of different size: 157 $\pm$ 38 mm^3 (in the shoulders), 67 $\pm$ 19 mm^3 (middle dorsolateral), and 27.8 $\pm$ 7.8 mm^3 (in the thighs).

Noninvasive PET imaging showed that [^{18}F]FEAU accumulation in the largest s.c. #4C6 tumors was heterogeneous and substantially higher in the central areas (peak levels of 1.44 $\pm$ 0.12% dose/g) as compared with that in the mid-sized tumors (peak levels of 1.02 $\pm$ 0.08% dose/g; average, 0.68 $\pm$ 0.34% dose/g) and small tumors (average, 0.12 $\pm$ 0.04% dose/g). These differences were statistically significant ($P < 0.05$; Student t test). Control C6 tumors did not accumulate [^{18}F]FEAU above the body background levels (0.02 $\pm$ 0.01% dose/g; Fig. 5*A*). The increase in [^{18}F]FEAU accumulation in the central regions of the largest #4C6 tumors reflects the presence of a hypoxic core.

Fluorescence macroscopic examination of excised tumors, which had been sectioned in planes similar to the PET images, revealed similarities in patterns of spatial heterogeneity and magnitude of HIF-1–mediated transcriptional activity. Namely, the largest #4C6 tumors had developed a hypoxic core, as evidenced by the irregular pattern of green fluorescence of hypoxia-induced reporter expression under macroscopic examination and matched the [^{18}F]FEAU PET image (Fig. 5*C* and *D*). GFP-fluorescing hypoxic tumor tissue was localized within and around the markedly hyperemic ring of tumor vasculature and around thrombosed larger vessels (Fig. 5*B* and *D*). These spotty-appearing perivascular hypoxic regions also were detectable on the PET images (Fig. 5*C* and *D*), albeit as medium-to-lower activity areas, reflecting the partial volume effect in the micro-PET images. In contrast, the periphery of the #4C6 reporter xenograft was well perfused and normoxic, as evidenced by bright red fluorescence of the constitutively expressed Red2XPRT reporter, the absence

of TKGFP fluorescence, and no PET signal. Fluorescence microscopic examination of these different areas at a cellular resolution confirmed these observations (Fig. 5*E–G*).

PET Imaging of HIF-1 Transcriptional Activity Induced by Ischemia-Reperfusion Injury. In the second group of mice ($n = 6$), two #4C6 tumors were established in both anterior paws and were allowed to grow up to 3 to 4 mm in diameter on each side (average volume, 24.1 $\pm$ 6.6 mm^3). The first microPET imaging study with [^{18}F]FEAU was performed to visualize the baseline level of TKGFP reporter expression. The level of [^{18}F]FEAU accumulation was low (average, 0.08 $\pm$ 0.03% dose/g) and similar in both tumor xenografts growing in the opposite paws (Fig. 6). Next day, acute ischemia-reperfusion injury in the left limb bearing a #4C6 xenograft was induced by 1-hour tourniquet application. The xenograft growing in the right paw served as a control. Repeat PET imaging performed 24 hours later revealed a substantially higher accumulation of [^{18}F]FEAU (1.41 $\pm$ 0.64% dose/g) in the tourniquet-treated xenografts than in the control xenografts (Fig. 6). This result showed a rapid induction of HIF-1 transcriptional activity in tumor tissue by an acute ischemia-reperfusion injury.

DISCUSSION

Currently, there are no PET radiotracers or MRI techniques that allow for noninvasive assessment of hypoxia-induced molecular-genetic and signaling processes in cells at transcriptional and post-transcriptional levels. Therefore, to study the temporal dynamics and spatial heterogeneity of hypoxia development and HIF-1–mediated transcriptional activation of hypoxia-inducible genes, we developed a novel HIF-1–specific reporter system that allows for noninvasive *in vivo* PET imaging in living mice. The Red2XPRT "beacon" gene (16) facilitates the imaging of transduced cell (tissue) localization, whereas the TKGFP "sensor" gene (19) allows for imaging of HIF-1 transcriptional activity. Furthermore, both reporter genes encode PET reporter enzymes (XPRT or HSV1-TK), which metabolically entrap specific radiolabeled probes (xanthine or FEAU) in transduced cells (16, 19). These enzymes are fused with fluorescent proteins (DsRed or eGFP) that allow for fluorescence microscopic visualization of expression of fusion reporter proteins in transduced cells *in vitro* and *in situ* and facilitate FACS-aided selection of transduced cells.

To achieve a tight HIF-1–specific regulation of TKGFP, we placed it under the control of eight repeats of an HRE derived from the
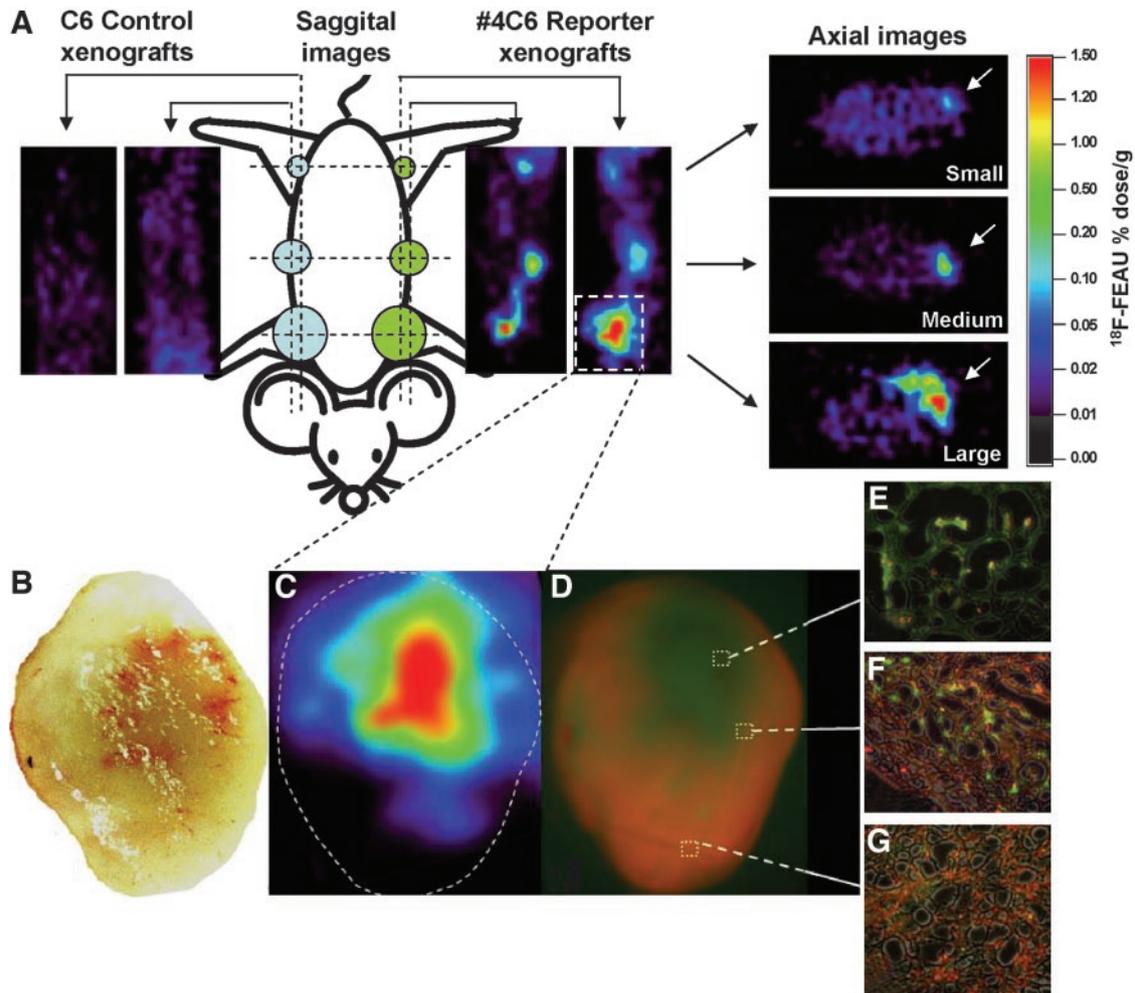
6105

Fig. 5. A. *In vivo* microPET imaging of HIF-1 transcriptional activity: tumor size dependency. [^{18}F]FEAU PET images of HIF-1 transcriptional activity (TKGFP expression) of a mouse bearing multiple wild-type C6 (control, *blue circles*) and #4C6 (reporter, *green circles*) tumor xenografts of different size (image planes are indicated by dotted lines continuing into solid arrows). Two sagittal image planes are shown through the #4C6-reporter xenografts (left side of animal + through wild-type C6 xenografts right side). Differently sized xenografts in the same animal provide simultaneous visualization of the central regions in each tumor and show a size-dependent magnitude and heterogeneity of hypoxia-induced HIF-1 transcriptional activity. Three axial PET images obtained through each pair C6 (control) and #4C6-reporter xenografts that are similar in size (growing on opposite sides) further show the heterogeneity of HIF-1–induced TKGFP expression. The dotted white square around the large #4C6 tumor defines the portion of the image used for *in vivo-in situ* comparison presented in *B–D*. Macrophotographic image (*B*) of the cut surface through the large #4C6 tumor shown in *C*; the cut surface was in a plane similar to the corresponding sagittal PET image (*A* and *C*); the tumor borders are outlined (*white dotted line*) based on the corresponding *macro* fluorescent image of the tumor (*D*). Fluorescence microscopic examination of these different areas at cellular resolution (×40 magnification) shows the hypervascular hypoxic core region (*E*), hypoxic-normoxic "border-zone" (*F*), and a normoxic region (*G*). One of the larger tumor vessels (located at the 9 o'clock position, *B*) was determined as thrombosed based on dissection microscopic examination. The hypoxic region adjacent to this thrombosed vessel is readily observable on the merged fluorescence image (*D*) and corresponding area on microPET image (*C*).

human *Epo* gene promoter. We decided not to use the full-length or partial VEGF or *Epo* gene promoters because they also harbor domains for regulation by other transcriptional activators (21). To facilitate the visualization of transduced cells, the Red2XPRT beacon reporter gene was placed under control of a constitutive CMV promoter downstream the TKGFP sensor gene. The dual reporter cassette was introduced into a self-inactivating retroviral vector that had a deletion in 3′-LTR (11).

The C6 rat glioma cell line was used in these studies because it is originally monoclonal and well characterized for hypoxia responsiveness, expresses high levels of inducible VEGF, and forms multicellular spheroids and solid tumors s.c. or intracerebrally in rats and nude mice (22–24). The functional characteristics of the resulting #4C6 cell line were assessed *in vitro* before proceeding with the *in vivo* imaging studies. We assessed the dynamic range and linearity of response of CoCl$_2$-induced inhibition of prolyl hydoxylase and the resulting activation of HIF-1 transcription by FACS-based measurements of TKGFP protein expression and by *in vitro* [^{14}C]FIAU radiotracer accumulation assay. A concentration-dependent linear response was

observed between 0 and 200 CoCl$_2$; concentrations >200 to 300 μmol/L induced significant cell toxicity and decreased cell population growth rate in agreement with previous reports (25).

Reduced atmospheric oxygen levels also induced an inverse concentration-dependent activation of HIF-1 transcription and up-regulation of TKGPF expression in #4C6 cells. The threshold level of TKGFP sensor gene induction was ~10% atmospheric oxygen; below this oxygen level TKGFP expression and enzymatic activity increased linearly. The comparison of CoCl$_2$ and low atmospheric oxygen-induced hypoxia models showed that chemically induced hypoxia was more effective in up-regulating HIF-1 transcriptional activity. The level of TKGFP expression induced by CoCl$_2$ was approximately twofold higher than that induced by 2% oxygen. This observation was further confirmed by measuring the levels of transcriptionally active HIF-1α complexes in #4C6 cells exposed for 24 hours to different CoCl$_2$ or atmospheric oxygen concentrations. Such difference in the magnitude of HIF-1 transcriptional inducibility by two hypoxia models could be explained, at least in part, by multiple compensatory adaptations in tumor cells in response to decreased intracellular pO$_2$
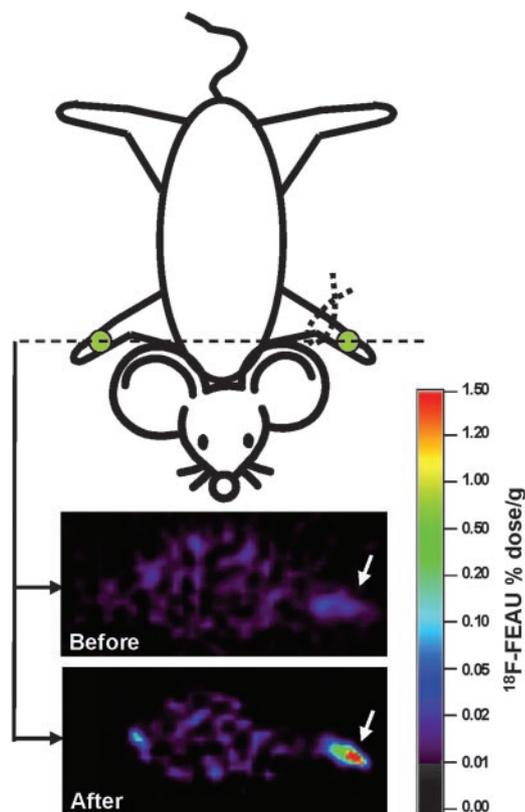
Fig. 6. *In vivo* microPET imaging of ischemia-reperfusion injury-induced HIF-1 transcriptional activity. Axial PET images of HIF-1–mediated TKGFP expression in s.c. #4C6 xenografts growing in both anterior limbs (*green circles*) of the same mouse before and after tourniquet application (*dotted knot*) to the left anterior limb proximally to tumor (*white arrow*). The s.c. #4C6 tumor xenograft growing in the right limb was not affected and served as a control.

and which may not occur or be more easily saturable with CoCl$_2$ (especially at higher CoCl$_2$ concentrations). This explanation is supported by results of our studies on temporal dynamics of CoCl$_2$-induced HIF-1α transcriptional complex formation. Increased concentrations of HIF-1α transcriptional complexes were detected as early as at 1 hour after chemically induced hypoxia. Then, at 4 hours after hypoxia induction, a surge in HIF-1 levels was observed, followed by a significant reduction of HIF-1 level by 24 hours of exposure to CoCl$_2$. Such pattern of temporal dynamics of HIF-1 transcriptional activity was observed at concentrations of CoCl$_2$ <200 μM. These results are consistent with reports of other investigators, who related Western blot analysis in the primary prostatic stromal cells showed the up-regulation (~10 fold) of HIF-1 at 4 hours with 100 μM and at 24 hours of treatment with 200 μM COCL$_2$ (26).

The next series of *in vitro* studies indicated that the rate of increase in numbers of TKGFP-expressing cells and the rate of VEGF secretion into the media by the same cell populations are similar. However, the magnitude of gene up-regulation was 10-fold higher for 8×HRE-TKGFP reporter as compared with endogenous VEGF. There are no other enhancer or repressor elements in our HIF-1α–specific reporter system besides 8×HRE, which could either positively or negatively affect TKGFP reporter expression under the baseline or hypoxia-induced conditions. In contrast, the baseline level of VEGF expression in C6 cells was relatively high even under normoxia and only moderately increased under hypoxic conditions.

Further, we used C6 reporter cells to study the temporal and size-dependent dynamics and spatial heterogeneity of hypoxia-induced HIF-1–mediated transcriptional activity in multicellular spheroids. We showed the emergence of hypoxic cells within the core of

spheroids when they grew >400 μm in diameter. In significantly larger spheroids (1 to 2 mm in diameter), a nonhypoxic shell surrounded a frankly hypoxic core. Other studies had shown that the threshold size at which the majority of multicellular spheroids grown from a variety of tumor cells develop a hypoxic core is ~400 to 500 μm (27). The thickness of the nonhypoxic spheroid shell estimated in the current study (~90 μm) is within the known 100-μm diffusion limit for oxygen and was comparable with that reported by other investigators (28).

A more detailed observation revealed the presence of occasional TKGFP-expressing cells in the peripheral cellular layers of large spheroids. One of many possible explanations of this phenomenon is that these peripherally located TKGFP-expressing cells may have originated in the hypoxic core but migrated into the nonhypoxic shell toward higher concentrations of oxygen and nutrients. Previous studies showed that when large C6 spheroids were embedded into collagen type I gel matrix, their central hypoxic cores released cells that had low proliferation but invaded the surrounding matrix at faster rates than the cells detached from the surface of small C6 spheroids (29).

MicroPET imaging revealed size-dependent differences in the magnitude and heterogeneity of HIF-1 transcriptional activity in #4C6 tumor xenografts. Small tumors (<30 mm^3) did not have a well-formed hypoxic core, as evidenced by low levels of [^{18}F]FEAU accumulation. This was not caused by partial volume effect in PET images because the fluorescence microscopy of the excised small #4C6 tumors showed only occasional TKGFP-expressing hypoxic cells and confirmed the absence of a well-formed hypoxic core. This observation contradicts the postulate that tumors initiate as avascular cell aggregates, then grow to sizes of ~1 to 3 mm^3 and remain dormant until becoming hypoxic, at which point they start producing proangiogenic factors and induce neoangiogenesis for additional tumor growth (30, 31).

Our results support the hypothesis that some microtumors developing in well-vascularized tissue can co-opt pre-existing host blood vessels, do not become hypoxic, and do not induce angiogenesis until reaching a much larger size. C6 gliomas and many other tumors constitutively secrete VEGF even under normoxia (32, 33). Therefore, it is conceivable that the constitutive expression rather than hypoxia-induced HIF-1–mediated up-regulation of VEGF triggers the induction neoangiogenesis during the early phases of tumor development. Such a mechanism of vascular recruitment previously was shown specifically in C6 gliomas (32), and a marked down-regulation of VEGF expression in C6 cells was achieved by constitutive expression of antisense VEGF that resulted in poorly vascularized and largely necrotic tumors (33).

In the current study, a significant spatial heterogeneity of HIF-1 transcriptional activity was imaged noninvasively with PET and confirmed by the comparative *in situ* microscopic analyses. Typically, large #4C6 tumors had a centrally located hypoxic core of an irregular shape surrounded by several asymmetrically located "satellite" hypoxic lesions. Not only the extent but also the magnitude of HIF-1 activation was several-fold higher in the hypoxic cores of large tumors as compared with that in medium-sized tumors. These hypoxic core regions manifested as areas of significantly higher levels of [^{18}F]FEAU accumulation and areas of higher TKGFP fluorescence intensity. The green-fluorescing (TKGFP-expressing) hypoxic tumor tissue was localized within and around the hyperemic ring of tumor vasculature (with markedly enlarged pathologic vessels) and around the thrombosed vessels. The hyperemic ring of tumor blood vessels detected within the peripheral zone of high HIF-1 transcriptional activity (TKGFP fluorescence) is consistent with the effects of VEGF that is overexpressed in this hypoxic tumor tissue. As shown by us and others (34, 35), the constitutive overexpression of VEGF in tumor

6107

tissue also causes hyperemia and the development of hemangioblastoma-like pathologically large blood vessels that are prone to thrombosis because of a sluggish blood flow that further contributes to hypoxia. Our observations are consistent with a recently reported study (32), which showed that the neovasculature of C6 tumors starts to undergo continuous microvascular remodeling when tumor size reaches several millimeters. This remodeling process involves not only the angiogenic sprouting but also was a spontaneous shutdown and consecutive regression of initially functional tumor vessel segments or even entire microvascular areas, which is analogous to ischemia-reperfusion injury.

To assess the role of HIF-1 signaling in ischemia-reperfusion injury in tumors and to image it, we developed tumor xenografts in both anterior paws in mice. The baseline PET imaging study showed the absence of hypoxia in the small-sized tumors. Thereafter, a moderate ischemia-reperfusion injury was induced in one of the tumors, and the PET imaging study was repeated. A significant up-regulation of HIF-1 transcription in the affected tumor as compared with the control tumor was observed consistent with a rapid induction of HIF-1 activity at 24 hours after reperfusion. These results are more dramatic than those observed using neonatal rat brain ischemia-reperfusion injury model, in which the levels of HIF-1 and VEGF peaked at 8 hours but declined significantly by 24 hours after injury, as showed by double-immunohistochemical staining of brain tissue sections (36). Therefore, our observations suggest that in contrast to normal tissue, C6 tumors are unable to rapidly compensate acute changes in tumor microcirculation.

In conclusion, repetitive PET imaging of HIF-1–specific reporter gene expression revealed that the constitutive oncogenic signaling rather than hypoxia-induced HIF-1 transcriptional activity plays a leading role in the induction of neoangiogenesis during the early phases of C6 tumor development. With the increase in C6 tumor size, a decompensation of blood flow and oxygen supply by the existing tumor vessels triggers a marked increase in HIF-1 transcriptional activity in the core regions of C6 tumors, which further promotes tumor neoangiogenesis. PET imaging also has shown that even a moderate ischemia-reperfusion injury in C6 tumors causes a rapid induction of HIF-1 transcriptional activity, which persists for a longer time than in normal tissues because of the inability of C6 tumors to rapidly compensate changes in tumor microcirculation. This PET imaging approach could be useful for repetitive noninvasive assessment of tumor hypoxia during preclinical development of novel radiation therapies and radiation sensitizers, antiangiogenic drugs, and different hypoxia-specific small molecular imaging agents.

REFERENCES

1. Wang GL, Semenza GL. Purification and characterization of hypoxia-inducible factor 1. J Biol Chem 1995;270:1230–7.
2. Salceda S, Caro J. Hypoxia-inducible factor 1α (HIF-1α) protein is rapidly degraded by the ubiquitin-proteasome system under normoxic conditions. Its stabilization by hypoxia depends on redox-induced changes. J Biol Chem 1997;272:22642–7.
3. Chan DA, Sutphin PD, Denko NC, Giaccia AJ. Role of prolyl hydroxylation in oncogenically stabilized hypoxia-inducible factor-1α. J Biol Chem 2002;277:40112–7.
4. Carrero P, Okamoto K, Coumailleau P, O'Brien S, Tanaka H, Poellinger R. Redox-regulated recruitment of the transcriptional coactivators CREB-binding protein and SRC-1 to hypoxia-inducible factor 1α. Mol Cell Biol 2000;20:402–15.
5. Wenger RH, Gassmann M. Oxygen(es) and the hypoxia-inducible factor-1. J Biol Chem 1997;378:609–16.
6. Kamura T, Koepp DM, Conrad MN, et al. Rbx1, a component of the VHL tumour suppressor complex and SCF ubiquitin ligase. Science 1999;284:657–61.
7. Fukuda R, Hirota K, Fan F, Jung YD, Ellis LM, Semenza GL. Insulin-like growth factor 1 induces hypoxia-inducible factor 1-mediated vascular endothelial growth factor expression, which is dependent on MAP kinase and phosphatidylinositol 3-kinase signaling in colon cancer cells. J Biol Chem 2002;277:38205–11.
8. Semenza GL. HIF-1: mediator of physiological and pathophysiological responses to hypoxia. J Appl Physiol 2000;88:1474–80.
9. Tjuvajev J, Stockhammer G, Desai R, et al. Imaging gene transfer and expression in vivo. Cancer Res 1995;55:6126–32.
10. Doubrovin M, Ponomarev V, Beresten T, et al. Imaging transcriptional regulation of p53 dependent genes with positron emission tomography in vivo. Proc Natl Acad Sci USA 2001;98:9300–5.
11. Ponomarev V, Doubrovin M, Lyddane C, et al. Imaging TCR-dependent NFAT-mediated T-cell activation with positron emission tomography in vivo. Neoplasia 2001;3:480–8.
12. Zhang L, Adams JY, Billick E, et al. Molecular engineering of a two-step transcription amplification (TSTA) system for transgene delivery in prostate cancer. Mol Ther 2002;5:223–32.
13. Luker GD, Luker KE, Sharma V, et al. In vitro and in vivo characterization of a dual-function green fluorescent protein–HSV1-thymidine kinase reporter gene driven by the human elongation factor 1 α promoter. Mol Imaging 2002;1:65–73.
14. Luker GD, Sharma V, Pica CM, et al. Noninvasive imaging of protein-protein interactions in living animals. Proc Natl Acad Sci USA 2002;99:6961–6.
15. Green LA, Yap CS, Nguyen K, et al. Indirect monitoring of endogenous gene expression by positron emission tomography (PET) imaging of reporter gene expression in transgenic mice. Mol Imaging Biol 2002;4:71–81.
16. Doubrovin M, Ponomarev V, Serganova I, et al. A new reporter gene system for molecular-genetic imaging of CNS with intact blood-brain barrier: bacterial xanthine phosphoribosyl transferase-radiolabeled xanthine. Mol Imaging 2003;2:93–112.
17. Ruan H, Su H, Hu L, Lamborn KR, Kan YW, Deen DF. A hypoxia-regulated adeno-associated virus vector for cancer-specific gene therapy. Neoplasia 2001;3:255–63.
18. Ory DS, Neugeboren BA, Mulligan RC. A stable human-derived packaging cell line for production of high titer retrovirus/vesicular stomatitis virus G pseudotypes. Proc Natl Acad Sci USA 1996;93:11400–6.
19. Jacobs A, Dubrovin M, Hewett J, et al. Functional coexpression of HSV-1 thymidine kinase and green fluorescent protein: implications for noninvasive imaging of transgene expression. Neoplasia 1999;1:154–61.
20. Alauddin MM, Shahinian A, Gordon EM, Bading JR, Conti PS. Preclinical evaluation of the penciclovir analog 9-(4-[(18)F]fluoro-3-hydroxymethylbutyl)guanine for in vivo measurement of suicide gene expression with PET. J Nucl Med 2001;42:1682–90.
21. Semenza GL, Jiang BH, Leung SW, et al. Hypoxia response elements in the aldolase A, enolase 1, and lactate dehydrogenase A gene promoters contain essential binding sites for hypoxia-inducible factor 1. J Biol Chem 1996;271:32529–37.
22. Plate KH, Breier G, Millauer B, Ullrich A, Risau W. Up-regulation of vascular endothelial growth factor and its cognate receptors in a rat glioma model of tumor angiogenesis. Cancer Res 1993;53:5822–7.
23. Acker H, Holtermann G, Bolling B, Carlsson J. Influence of glucose on metabolism and growth of rat glioma cells (C6) in multicellular spheroid culture. Int J Cancer 1992;52:279–85.
24. Tamaki M, McDonald W, Amberger VR, Moore E, Del Maestro RF. Implantation of C6 astrocytoma spheroid into collagen type I gels: invasive, proliferative, and enzymatic characterizations. J Neurosurg 1997;87:602–9.
25. Zou W, Zeng J, Zhuo M, et al. Involvement of caspase-3 and p38 mitogen-activated protein kinase in cobalt chloride-induced apoptosis in PC12 cells. J Neurosci Res 2002;67:837–43.
26. Berger AP, Kofler K, Bektic J, et al. Increased growth factor production in a human prostatic stromal cell culture model caused by hypoxia. Prostate 2003;57:57–65.
27. Groebe K, Mueller-Klieser W. On the relation between size of necrosis and diameter of tumor spheroids. Int J Radiat Oncol Biol Phys 1996;34:395–401.
28. Kunz-Schughart LA, Doetsch J, Mueller-Klieser W, Groebe K. Proliferative activity and tumorigenic conversion: impact on cellular metabolism in 3-D culture. Am J Physiol Cell Physiol 2000;278:C765–80.
29. Tamaki M, McDonald W, Amberger VR, Moore E, Del Maestro RF. Implantation of C6 astrocytoma spheroid into collagen type I gels: invasive, proliferative, and enzymatic characterizations. J Neurosurg 1997;87:602–9.
30. Folkman J. Tumor angiogenesis: therapeutic implications. N Engl J Med 1971;285:1182–6.
31. Hanahan D, Folkman J. Patterns and emerging mechanisms of the angiogenic switch during tumorigenesis. Cell 1996;86:353–64.
32. Vajkoczy P, Farhadi M, Gaumann A, et al. Microtumor growth initiates angiogenic sprouting with simultaneous expression of VEGF, VEGF receptor-2, and angiopoietin-2. J Clin Investig 2002;109:777–85.
33. Saleh M, Stacker SA, Wilks AF. Inhibition of growth of C6 glioma cells in vivo by expression of antisense vascular endothelial growth factor sequence. Cancer Res 1996;56:393–401.
34. Oku T, Tjuvajev JG, Miyagawa T, et al. Tumor growth modulation by sense and antisense vascular endothelial growth factor gene expression: effects on angiogenesis, vascular permeability, blood volume, blood flow, fluorodeoxyglucose uptake, and proliferation of human melanoma intracerebral xenografts. Cancer Res 1998;58:4185–92.
35. Johansson M, Brannstrom T, Bergenheim AT, Hemriksson R. Spatial expression of VEGF-A in human glioma. J Neurooncol 2002;59:1–6.
36. Mu D, Jiang X, Sheldon RA, et al. Regulation of hypoxia-inducible factor 1α and induction of vascular endothelial growth factor in a rat neonatal stroke model. Neurobiol Dis 2003;14:524–34.

Molecular Imaging of Temporal Dynamics and Spatial Heterogeneity of Hypoxia-Inducible Factor-1 Signal Transduction Activity in Tumors in Living Mice

Inna Serganova, Michael Doubrovin, Jelena Vider, et al.

Updated version	Access the most recent version of this article at: http://cancerres.aacrjournals.org/content/64/17/6101

Cited articles	This article cites 33 articles, 15 of which you can access for free at: http://cancerres.aacrjournals.org/content/64/17/6101.full#ref-list-1
Citing articles	This article has been cited by 35 HighWire-hosted articles. Access the articles at: http://cancerres.aacrjournals.org/content/64/17/6101.full#related-urls

E-mail alerts	Sign up to receive free email-alerts related to this article or journal.
Reprints and Subscriptions	To order reprints of this article or to subscribe to the journal, contact the AACR Publications Department at pubs@aacr.org.
Permissions	To request permission to re-use all or part of this article, use this link http://cancerres.aacrjournals.org/content/64/17/6101. Click on "Request Permissions" which will take you to the Copyright Clearance Center's (CCC) Rightslink site.